Iranian Journal of Science & Technology, Transaction B, Vol. 28, No. B5
Printed in The Islamic Republic of Iran, 2004

SECOND-ORDER CLOSURE STUDY OF RIVER-HARBOUR FLOW*

H. HAKIMZADEH
Faculty of Civil Engineering, Sahand University of Technology, Tabriz, P.O.Box 51335/1996, I.R. of Iran
Email: hakimzadeh@sut.ac.ir

Abstract– A complete second-order closure model of turbulence has been used to predict the behaviour of fully developed turbulent flow in a square river harbour. For the two dimensional, this closure model entails the solution of five differential equations for the turbulence parameters, excluding the three general equations of motion. The turbulent flow was driven by a stationary current in an adjacent model river. Emphasis has been focused on comparing the simple and more sophisticated turbulence models, including the Reynolds and algebraic stress models to predict accurately the velocity patterns within such basins. The governing equations have been discretized using the finite difference method. The advective acceleration terms in the hydrodynamics equations were treated using the third order upwind scheme, whereas the counterpart terms in the k-ε equations were treated using the exquisite scheme. Experimental data from the model river harbour were used to check the numerical model results, which found that both of the closure models of turbulence generally produced accurate results for the tests considered within the harbour.

Keywords– River harbour, turbulent flow, depth integrated model, Reynolds stress model, boundary conditions

1. INTRODUCTION

The harbours situated along rivers and estuaries usually suffer from siltation of their basins. Removal and disposal of sediments deposited in harbour basins often involve high costs, particularly when the sediment is contaminated with micro-pollutants that are adsorbed on the clay and silt particles. The siltation of a harbour results from a net transport of sediments into the harbour which is caused by the often quite complicated flow patterns in the harbour entrance. Since the siltation process mainly depends on the flow pattern, the determination of the velocity field within such basins will be an important issue. Software tools are now available to determine the flow pattern within such basins. A major requirement of these tools is that they accurately predict the circulation pattern within such basins before proceeding to predict the sedimentation process. However, such models are generally used for marina planning and are therefore rarely calibrated and verified against prototype data. On the other hand, the circulation patterns in harbour entrances driven by steady river flows have been extensively examined in the laboratory by a number of researchers including [1-5]. In the current study, the data from experiments carried out by the hydromechanics group of the civil engineering faculty at the Delft University of Technology, Langendoen [6], (cited in Bijvelds *et al*. [7]) were used for model verification. These measurements pertained to a stationary and homogeneous free surface cavity flow in a 1×1 m^2 harbour. The flow in this model harbour was driven by a river discharge Q of $0.042 m^3/s$; the water depth d was equal to 0.11 m in still water; and the width of the river was 1 m. The actual model river length was 18 m, however as in Bijvelds *et al.* [7], the computational model river length was set to be $5m$. The sidewalls of the model were vertical.

The numerical model results based on using the mixing length and the k-ε model have already been compared with measured data and the k-ε model results were found to be in good agreement with the laboratory data [8]. For the numerical model reported herein however, the second-order closure models of

*Received by the editors March 10, 2003 and in final revised form July 25, 2004

turbulence, including the Reynolds and algebraic stress models have been used to predict the circulation pattern in a square river harbour (see Fig. 1).

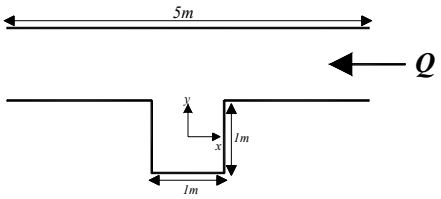

Fig. 1. Configuration of the computational model harbour and river

2. DEPTH-INTEGRATED HYDRODYNAMIC EQUATIONS

The equations of motion for a two-dimensional depth-averaged flow are best obtained by integrating the three-dimensional Reynolds equations over the depth. Assuming that the vertical acceleration is negligible compared to gravity, the continuity and horizontal momentum equations can be derived as given by ASCE Task Committee [9]

$$\frac{\partial \zeta}{\partial t}+\frac{\partial UH}{\partial x}+\frac{\partial VH}{\partial y}=0 \tag{1}$$

$$\frac{\partial UH}{\partial t}+\beta\left[\frac{\partial U^2H}{\partial x}+\frac{\partial UVH}{\partial y}\right]=f_cVH-gH\frac{\partial \zeta}{\partial x}+\frac{C_s\rho_aW_xW_s}{\rho}$$

$$-\frac{gUV_s}{C^2}+\frac{\partial(-\overline{u'u'})H}{\partial x}+\frac{\partial(-\overline{u'v'})H}{\partial y} \tag{2}$$

$$\frac{\partial VH}{\partial t}+\beta\left[\frac{\partial UVH}{\partial x}+\frac{\partial V^2H}{\partial y}\right]=-f_cUH-gH\frac{\partial \zeta}{\partial y}+\frac{C_s\rho_aW_yW_s}{\rho}$$

$$-\frac{gVV_s}{C^2}+\frac{\partial(-\overline{v'u'})H}{\partial x}+\frac{\partial(-\overline{v'v'})H}{\partial y} \tag{3}$$

where ζ = water surface elevation above (positive) datum (h), t=time, x,y=Cartesian co-ordinates in the horizontal plane, U,V = depth averaged velocity components in the x,y directions, H=total depth ($\zeta+h$), β= momentum correction factor, f_c =Coriolis parameter ($=2\varpi\sin\phi$, where ϖ=speed of earth's rotation and ϕ= earth's latitude), g=gravity, C_s =air-water resistance coefficient, ρ_a=air density, ρ=fluid density, W_x and W_y =wind velocity components in x and y directions respectively, W_s = wind speed, C=Chezy bed friction factor, V_s =depth averaged fluid speed ($=\sqrt{U^2+V^2}$) and $-\overline{u_i'u_j'}$ = depth averaged Reynolds stresses.

Assuming that the velocity profile in the vertical plane can be adequately represented by a logarithmic distribution, the value of correction factor β for the non-uniformity of the velocity profile becomes

$$\beta\cong 1+g/\kappa^2C^2 \tag{4}$$

where κ=von Karman's constant (=0.4). The Coriolis parameter and wind stress were not included in the current study.

3. TURBULENCE MODELS

For the second-order closure of turbulence, the modified depth integrated equations for the Reynolds stresses proposed by Launder *et al*. [10] have been used to determine the unknown stresses. Then, by making the local equilibrium assumption (i.e. $P=\varepsilon$), these equations can be reduced to the following forms [11]:

$$\frac{\partial \overline{u'u'}H}{\partial t}+\frac{\partial \overline{u'u'}UH}{\partial x}+\frac{\partial \overline{u'u'}VH}{\partial y}=\frac{\partial}{\partial x}\left(C_k\frac{\bar{k}^2H}{\bar{\varepsilon}}\cdot\frac{\partial \overline{u'u'}}{\partial x}\right)+\frac{\partial}{\partial y}\left(C_k\frac{\bar{k}^2H}{\bar{\varepsilon}}\cdot\frac{\partial \overline{u'u'}}{\partial y}\right)$$

$$-2(1-c_2)\left[\overline{u'u'}H\left(\frac{\partial U}{\partial x}\right)+\overline{u'v'}H\left(\frac{\partial U}{\partial y}\right)-P_{kv}H\right]-c_1\frac{\bar{\varepsilon}}{\bar{k}}\overline{u'u'}H-\frac{2}{3}(1-c_1-c_2)\bar{\varepsilon}H \tag{5}$$

$$\frac{\partial \overline{v'v'}H}{\partial t}+\frac{\partial \overline{v'v'}UH}{\partial x}+\frac{\partial \overline{v'v'}VH}{\partial y}=\frac{\partial}{\partial x}\left(C_k\frac{\bar{k}^2H}{\bar{\varepsilon}}\cdot\frac{\partial \overline{v'v'}}{\partial x}\right)+\frac{\partial}{\partial y}\left(C_k\frac{\bar{k}^2H}{\bar{\varepsilon}}\cdot\frac{\partial \overline{v'v'}}{\partial y}\right)$$

$$-2(1-c_2)\left[\overline{u'v'}H\left(\frac{\partial V}{\partial x}\right)+\overline{v'v'}H\left(\frac{\partial V}{\partial y}\right)-P_{kv}H\right]-c_1\frac{\bar{\varepsilon}}{\bar{k}}\overline{v'v'}H-\frac{2}{3}(1-c_1-c_2)\bar{\varepsilon}H \tag{6}$$

$$\frac{\partial \overline{u'v'}H}{\partial t}+\frac{\partial \overline{u'v'}UH}{\partial x}+\frac{\partial \overline{u'v'}VH}{\partial y}=\frac{\partial}{\partial x}\left(C_k\frac{\bar{k}^2H}{\bar{\varepsilon}}\cdot\frac{\partial \overline{u'v'}}{\partial x}\right)+\frac{\partial}{\partial y}\left(C_k\frac{\bar{k}^2H}{\bar{\varepsilon}}\cdot\frac{\partial \overline{u'v'}}{\partial y}\right)$$

$$-(1-c_2)\left[\overline{u'u'}H\left(\frac{\partial V}{\partial x}\right)+\overline{u'v'}H\left(\frac{\partial U}{\partial x}+\frac{\partial V}{\partial y}\right)+\overline{v'v'}H\left(\frac{\partial U}{\partial y}\right)\right]-c_1\frac{\bar{\varepsilon}}{\bar{k}}\overline{u'v'}H \tag{7}$$

where $\bar{k}$ = depth averaged turbulent kinetic energy, $\bar{\varepsilon}$ = depth averaged dissipation rate of turbulent kinetic energy, $P_{kv}=c_k U_*^3/H$, $U_*=c_f(U^2+V^2)^{1/2}$ = bed shear velocity, c_f = friction coefficient $(=\sqrt{g}/C)$, $c_k=c_f^{-1/2}$, $c_1=2.2, c_2=0.55$ and $C_k=0.09$.

For the sake of simplicity, the depth integrated standard *k*-ε equations have been used to calculate the required turbulent kinetic energy and dissipation rate [12]

$$\frac{\partial \bar{k}H}{\partial t}+\frac{\partial \bar{k}UH}{\partial x}+\frac{\partial \bar{k}VH}{\partial y}=\frac{\partial}{\partial x}\left(\frac{\bar{\nu}_t H}{\sigma_k}\cdot\frac{\partial \bar{k}}{\partial x}\right)+\frac{\partial}{\partial y}\left(\frac{\bar{\nu}_t H}{\sigma_k}\cdot\frac{\partial \bar{k}}{\partial y}\right)$$

$$-\left[\overline{u'v'}H\left(\frac{\partial U}{\partial y}+\frac{\partial V}{\partial x}\right)+\overline{u'u'}H\left(\frac{\partial U}{\partial x}\right)+\overline{v'v'}H\left(\frac{\partial V}{\partial y}\right)\right]+c_kU_*^3-\bar{\varepsilon}H \tag{8}$$

$$\frac{\partial \bar{\varepsilon}H}{\partial t}+\frac{\partial \bar{\varepsilon}UH}{\partial x}+\frac{\partial \bar{\varepsilon}VH}{\partial y}=\frac{\partial}{\partial x}\left(\frac{\bar{\nu}_t H}{\sigma_\varepsilon}\cdot\frac{\partial \bar{\varepsilon}}{\partial x}\right)+\frac{\partial}{\partial y}\left(\frac{\bar{\nu}_t H}{\sigma_\varepsilon}\cdot\frac{\partial \bar{\varepsilon}}{\partial y}\right)$$

$$-c_{1\varepsilon}\frac{\bar{\varepsilon}}{\bar{k}}\left[\overline{u'u'}H\left(\frac{\partial U}{\partial x}\right)+\overline{v'v'}H\left(\frac{\partial V}{\partial y}\right)+\overline{u'v'}H\left(\frac{\partial U}{\partial y}+\frac{\partial V}{\partial x}\right)\right]+c_\varepsilon\frac{U_*^4}{H}-c_{2\varepsilon}\frac{\bar{\varepsilon}^2}{\bar{k}}H \tag{9}$$

where $\bar{\nu}_t(=c_\mu\bar{k}^2/\bar{\varepsilon})$ = depth averaged turbulent eddy viscosity, $c_\varepsilon=3.6c_{2\varepsilon}c_\mu^{1/2}c_f^{-3/4}$ and $\sigma_k=1.0$, $\sigma_\varepsilon=1.3$, $c_\mu=0.09$, $c_{1\varepsilon}=1.44$, $c_{2\varepsilon}=1.92$ are standard constant coefficients of the *k*-ε equations.

Although different lower values for the vertical production coefficients of bed turbulence were suggested by Booij [13] and Hakimzadeh [11], for the current study the standard values of these coefficients were used as given by Rodi [14] and applied by Falconer and Li [12].

For the depth integrated algebraic stress model, the simplified Reynolds stresses have been represented as [15]

$$-\overline{u'u'}=2A^2B\left(\frac{\partial U}{\partial y}\right)^2-2AP_{kv}+B,\ -\overline{v'v'}=2A^2B\left(\frac{\partial V}{\partial x}\right)^2-2AP_{kv}+B,\ -\overline{u'v'}=-AB\left(\frac{\partial U}{\partial y}+\frac{\partial V}{\partial x}\right) \tag{10}$$

where $A = \frac{1-c_2}{c_1} \cdot \frac{\bar{k}}{\bar{\varepsilon}}$, $B = \frac{2\bar{k}}{3} \cdot \frac{1-c_1-c_2}{c_1}$.

Also in using the widely accepted eddy viscosity concept, both for the *k*-ε and mixing length turbulence models, the Reynolds stresses for each component read

$$-\overline{u'u'} = 2\bar{\nu}_t\left(\frac{\partial U}{\partial x}\right) - \frac{2}{3}\bar{k}, \quad -\overline{v'v'} = 2\bar{\nu}_t\left(\frac{\partial V}{\partial y}\right) - \frac{2}{3}\bar{k}, \quad -\overline{u'v'} = \bar{\nu}_t\left(\frac{\partial V}{\partial x} + \frac{\partial U}{\partial y}\right) \tag{11}$$

Then for the *k*-ε model, Eqs. (8) and (9) were used to calculate the eddy viscosity coefficients, whereas for the mixing length model the proposed equation of Fischer [16] was used for this purpose

$$\bar{\nu}_t = 0.15 U_* H \tag{12}$$

4. BOUNDARY CONDITIONS

In the numerical model, the river flow boundaries were treated as open flow boundaries, with the river discharge was to be $0.042 m^3/s$. For an open boundary, an inflow boundary condition was prescribed for the turbulent parameters [14]

$$-\overline{u_i' u_j'} = \bar{k} = \bar{\varepsilon} = 0 \tag{13}$$

Further details of the open boundaries will be discussed in the section of model results. For the turbulent parameters *k* and ε along a solid wall normal to the *x*-direction, the following assumptions have been used [12]

$$\frac{\partial \bar{k}}{\partial x} = 0 \text{ and } \frac{\partial \bar{\varepsilon}}{\partial x} = 0 \tag{14}$$

The turbulent characteristics adjacent to solid boundaries are calculated using a wall function approach [12], whereby

$$\bar{k}_w = \frac{U_*^2}{c_\mu^{1/2}}, \quad \bar{\varepsilon}_w = \frac{U_*^3}{\kappa z_c} \tag{15}$$

where z_c = distance from solid boundary and U_* = wall shear velocity. For the Reynolds stresses, these quantities were set to be shear stress adjacent to the wall, as proposed by Jaw and Chen [17].

5. NUMERICAL METHOD

In solving the governing equations, an alternating direction implicit finite difference scheme has been used, including a refined and more accurate space staggered grid scheme where depths are included at the centre of the grid sides. A rectangular grid with a cell size of $25mm \times 25mm$ was chosen, with the computational domain therefore containing 200×82 grid cells. The difference equations were fully centered in both time and space, with the advective acceleration and the turbulent diffusion terms being centered by iteration. The difference scheme had no stability constraints, although it was established that the accuracy of the scheme deteriorated rapidly when the Courant number exceeded eight. In the finite difference equations, particular attention was paid to the treatment of the advective acceleration terms, with these terms being of considerable importance in modelling re-circulating flows. The components of the advective accelerations were represented in their pure differential form, thereby conserving momentum precisely in the difference scheme. Furthermore, these terms were represented using the higher order accurate third order upwind scheme, which eliminates the introduction of numerical diffusion and minimizes grid scale oscillations [8]. On the other hand, the counterpart terms in the depth integrated *k*-ε equations were represented using the exquisite scheme, as proposed by Leonard [18].

6. MODEL RESULTS AND COMPARISONS

At the upper open boundaries the rate of flow started from zero, increased on a sine curve up to a certain value (i.e. the river discharge) and then remained constant. The lower boundary was set to be either the open flow or water elevation boundary. Also, the sensitivity of the type of lower boundary has been studied carefully and it was found that the numerical model results and circulation patterns within the river harbour remained almost unchanged. Therefore, a circulation cell grew rapidly in strength and shape within the model harbour and then became stable.

The measurement data and computational open boundary conditions used in the current study were the same as outlined by Bijvelds *et al*. [7]. The predicted numerical model results of the mixing length and *k*-ε turbulence models in using various closed boundary conditions have already been compared with the measured data and the *k*-ε turbulence was found to be in good agreement with the laboratory data [8].

However, for the numerical model predictions reported herein, the flow patterns were almost similar within the basin in using the algebraic and Reynolds stress turbulence models and the large eddy dominated within the model harbour. The predicted circulation pattern within the harbour using the Reynolds and algebraic stress turbulence models are shown in Fig. 2. As can be seen from the figures, the predicted circulation cell of both models seems to be more accurate when compared with that of the mixing length model [8]. For the current tests, the Reynolds and algebraic stress turbulence models have correctly predicted the large eddy, which is in good agreement with the laboratory measurements. Also, the predicted turbulent kinetic energy distributions using the Reynolds and algebraic stress turbulence models within the basin are shown in Figs. 3a and 3b. The main structure of these distributions is almost similar. However, the predicted numerical results of application of the algebraic stress model are slightly greater than those of the Reynolds stress model. These similarities can also be seen in the predicted numerical model results of the normal Reynolds stresses using the Reynolds and algebraic stress turbulence models within the basin, as shown in Figs. 4 and 5.

Another typical example of comparisons between the measured and numerically predicted results for the different turbulence models are illustrated in Figs. 6a and 6b, where the '*V* ' and '*U*' velocity profiles across the two main axes are shown respectively. Also, for this section, in order to compare the model results of the all time-averaged types of closure models, the numerical model results of the *k*-ε and simple mixing length turbulence models are included in the figures. As can be seen from these comparisons, the predicted velocity values of the three sophisticated turbulence models (i.e. the Reynolds stress, algebraic stress and *k*-ε) were in very good agreement with the experimental data. In comparing all of the velocity results it was found that except for the mixing length model, the second order closure models and the *k*-ε model of the eddy viscosity concept generally produced accurate results for the tests considered.

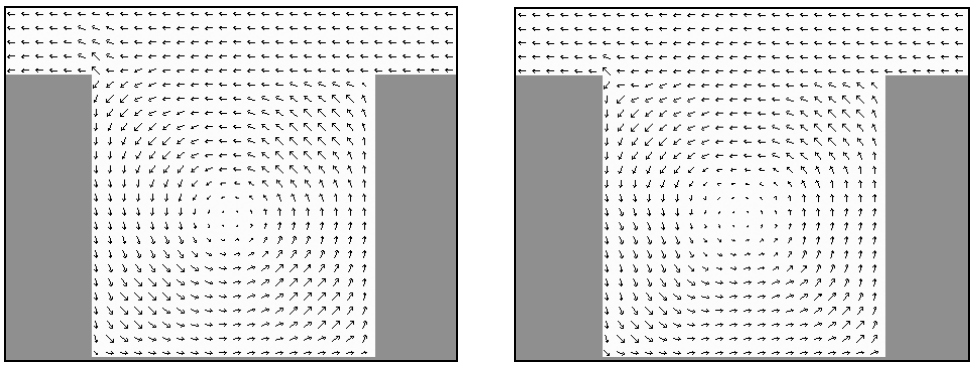

a) Reynolds stress model b) Algebraic stress model

Fig. 2. Flow pattern within the river harbour using the second order closure models

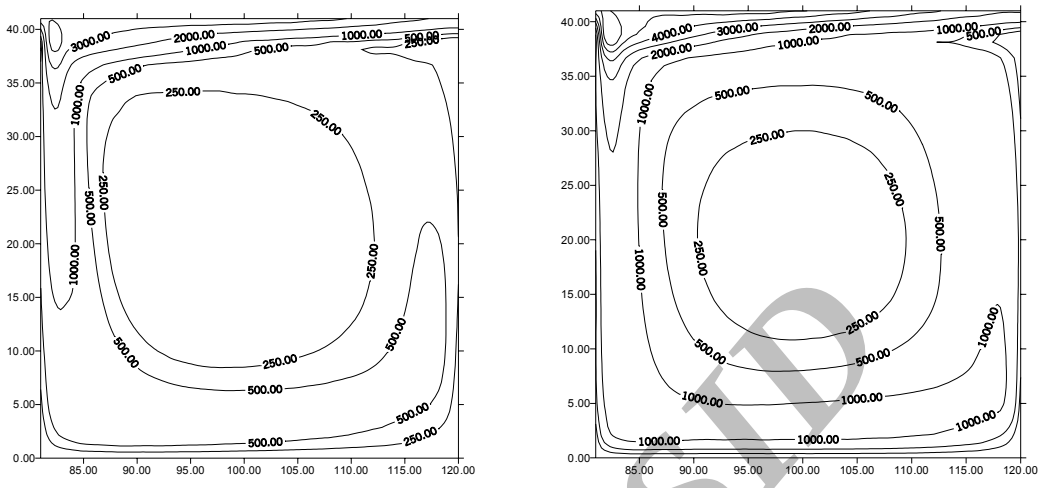

a) Reynolds stress model b) Algebraic stress model

Fig. 3. Turbulent kinetic energy distributions using the second order closure models (mm^2/s^2)

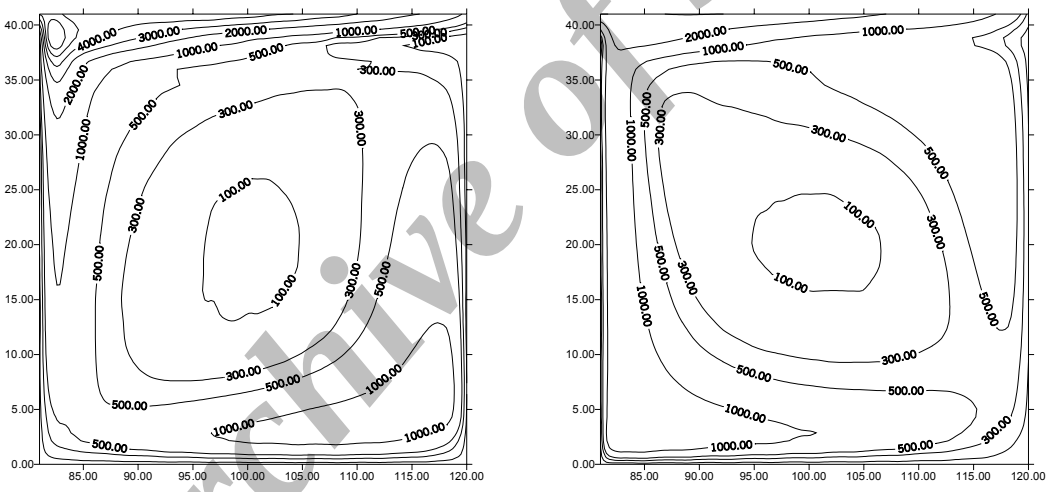

a) Normal Reynolds stress distribution in x-direction ($\overline{u'u'}$) b) Normal Reynolds stress distribution in y-direction ($\overline{v'v'}$)

Fig. 4. Normal Reynolds stresses distributions using the algebraic stress model (mm^2/s^2)

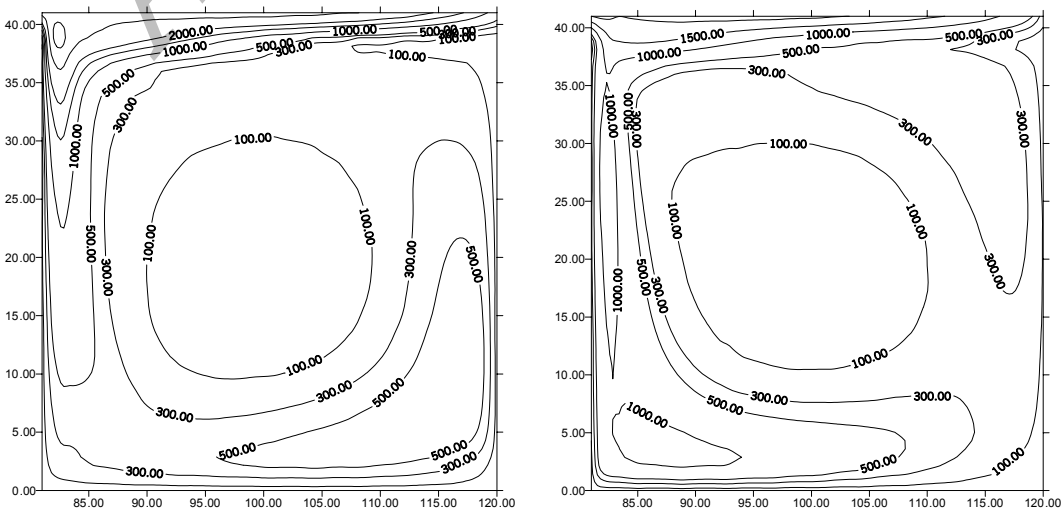

a) Normal Reynolds stress distribution in x-direction ($\overline{u'u'}$) b) Normal Reynolds stress distribution in y-direction ($\overline{v'v'}$)

Fig. 5. Normal Reynolds stress distribution using the Reynolds stress model (mm^2/s^2)

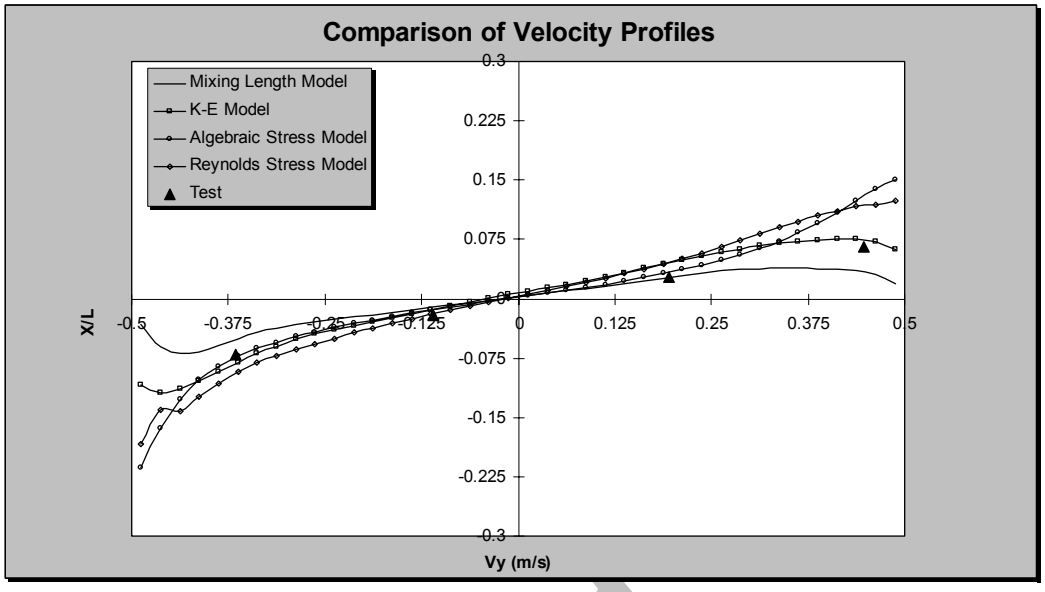

Fig. 6a. Comparison of velocity profile across the *x* axis

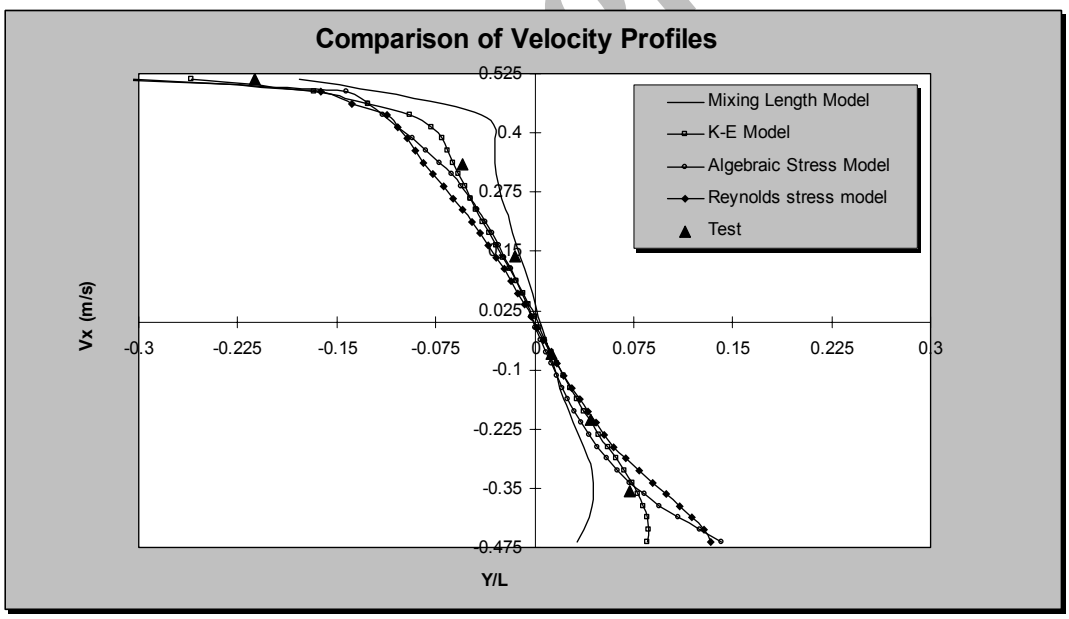

Fig. 6b. Comparison of velocity profile across the *y* axis

7. CONCLUSION

Details are given of an extensive on-going research programme to predict more accurately the circulation cell within river harbours. In the study reported herein, the numerical model results of the second order turbulence models, including the Reynolds and algebraic stress models, *k*-ε and mixing length models have been compared with the experimental data within the river harbour. The findings from this study have shown that the numerical results of the second order closure and *k*-ε models have reproduced the circulation cell and the velocity field very accurately for the harbour. These models are therefore recommended for modelling cavity turbulent flow and circulation patterns in marinas and harbours. Although the turbulent kinetic energy, normal Reynolds stresses distributions and velocity field predictions obtained using the algebraic and Reynolds stress turbulence models were slightly different, the computational effort required for the latter was almost twice that of the previous one.

Acknowledgements- The numerical model study presented herein is based on the final results of an ongoing research programme funded by Sahand University of Technology in the Islamic Republic of Iran. The author received a great deal of assistance from the research committee of the university and is grateful for their co-operation.

NOMENCLATURE

ζ	water surface elevation above (positive) datum
t	time
x,y	Cartesian co-ordinates in horizontal plane
U,V	depth averaged velocity components in x,y directions
H	total depth
β	momentum correction factor
f_c	Coriolis parameter (= $2\varpi \sin\phi$)
ϖ	speed of earth's rotation
ϕ	earth's latitude
g	gravity
C_s	air-water resistance coefficient
ρ_a	air density
ρ	fluid density
W_x, W_y	wind velocity components in x , y directions respectively
W_s	wind speed
C	Chezy bed friction factor
V_s	depth averaged fluid speed
$-\overline{u_i' u_j'}$	the Reynolds stresses
κ	von Karman's constant
$\bar{k}$	turbulent kinetic energy
$\bar{\varepsilon}$	dissipation rate of turbulent kinetic energy
$\bar{\nu}_t$	turbulent eddy viscosity
$\sigma_k, \sigma_\varepsilon$	constant coefficients
c_μ	constant coefficients
$c_{1\varepsilon}, c_{2\varepsilon}$	constant coefficients
c_f	friction coefficient
c_k	$c_f^{-1/2}$
c_ε	$3.6 c_{2\varepsilon} c_\mu^{1/2} c_f^{-3/4}$
A	$\frac{1-c_2}{c_1} \cdot \frac{\bar{k}}{\bar{\varepsilon}}$
B	$\frac{2\bar{k}}{3} \cdot \frac{1-c_1-c_2}{c_1}$
P_{kv}	$c_k \frac{U_*^3}{H}$
c_1, c_2	constant coefficients
$\bar{k}_w$	turbulent kinetic energy adjacent to the wall
$\bar{\varepsilon}_w$	dissipation rate of turbulent kinetic energy adjacent to the wall
U_*	wall shear velocity
z_c	distance from solid boundary

REFERENCES

1. Jiang, J. X. & Falconer, R. A. (1985). The influence of entrance conditions and Longshore currents on tidal flushing and circulation in model rectangular harbours. *Proceedings of International Conference on Numerical and Hydraulic Modelling of Ports and Harbours,* 65-74, Birmingham, England.
2. Jodan, S. A. & Regab, S. A. (1994). On the unsteady and turbulent characteristics of the three dimensional shear-driven cavity flow. *Journal of Fluid Engineering, Transaction of the ASME, 116*(3), 439-449.
3. Langendoen, E. J., Kranenburg, C. & Booij, R. (1994). Flow patterns and exchange of matter in tidal harbours. *Journal of Hydraulic Research, 32*(2), 259-270.
4. Nece, R. E. (1984). Planform effects on tidal flushing of marinas. *Journal of Waterway, Port, Coastal and Ocean Eng., ASCE, 110*(2), 251-269.
5. Zhou, J. G. (1995). Velocity-depth coupling in shallow-water flows. *Journal of Hydraulic Engineering, 121*(10), 717-724.
6. Langendoen, E. J. (1992). Flow patterns and transport of dissolved matter in tidal harbours. PhD Thesis, Delft University of Technology, Delft, The Netherlands.
7. Bijvelds, M. D. J. P., Kranenburg, C. & Stelling, G. S. (1999). 3D Numerical simulation of turbulent shallow-water flow in square harbour. *Journal of Hydraulic Engineering., 125*(1), 26-31.
8. Hakimzadeh, H. (2002). Simulation of water circulation in river harbours using zero and two-equation turbulence models. *Journal of Faculty of Engineering*, No. 27, University of Tabriz, 1-12.
9. ASCE Task Committee on Turbulence Models in Hydraulic Computations. (1988). Turbulence modelling of surface water flow and transport: Part I. *Journal of Hydraulic Engineering*, *114*(6), 970-991.
10. Launder, B. E., Reece, G. J. & Rodi, W. (1975). Progress in the development of a Reynolds stress turbulence closure. *Journal of Fluid Mechanics*, *68*, 537-566.
11. Hakimzadeh, H. (1997). Turbulence modelling of tidal currents in rectangular harbours. PhD Thesis, University of Bradford, Bradford, UK.
12. Falconer, R. A. & Li, G. (1994). Numerical modelling of tidal eddies in coastal basins with narrow entrances using the k-ε turbulence model. *Mixing and Transport in the Environment*, eds. K. J. Beven, *et al*., John Wiley & Sons Ltd., London, 325-350.
13. Booij, R. (1989). Depth-averaged *k*-ε modelling. *Proceedings of XXIIIth IAHR Congress,* A119-A206, Ottawa.
14. Rodi, W. (1984). *Turbulence models and their application in hydraulics*. *IAHR*, Second Edition, Delft, Netherlands, 1-104.
15. Hakimzadeh, H. & Falconer, R. A. (1997). Turbulence modelling of secondary tide induced circulation in rectangular harbours. *Proceedings of 27th IAHR Congress, ed. Sam S.Y. Wang,* ASCE Publications, *1*, 785-790.
16. Fischer, H. B. (1973). Longitudinal dispersion and turbulent mixing in open channel flow. *Annual Review of Fluid Mechanics, 5*, 59-78.
17. Jaw, S. Y. & Chen, C. J. (1998). Present status of second-order closure turbulence models. II Applications. *Journal of Engineering Mechanics, 124*(5), 502-512.
18. Leonard, B. P. (1988). Simple high-accuracy resolution program for convective modelling of discontinuities. *International Journal for Numerical Methods in Fluids*, John Wiley & Sons Ltd, 8, 1291-1318.